

## SCATTERING MORPHOLOGY RESOLVED TOTAL INTERNAL REFLECTION MICROSCOPY (SMR-TIRM) OF COLLOIDAL SPHERES

J. Yan,<sup>1</sup> D. S. Efremenko,<sup>2</sup> A. A. Vasilyeva,<sup>3</sup> A. Doicu,<sup>2</sup>  
T. Wriedt,<sup>4</sup> and C. Wirth<sup>5,6</sup>

Nanometer to micrometer scale colloidal particles are regularly found in applications in which surface forces dominate behavior. Consequently, a wide range of surface force measurement tools have been developed to probe interactions as a function of physiochemical properties. One tool, Total Internal Reflection Microscopy (TIRM), is an exceptionally sensitive probe of both conservative and non-conservative surface forces. A recent variant of TIRM called Scattering Morphology Resolved (SMR) TIRM utilizes the morphology of scattered light in concert with the integrated intensity to measure the position and orientation of a colloidal particle. Although the target of SMR-TIRM is the field of non-spherical “anisotropic” particles, spherical particles have been found to scatter evanescent waves with surprising morphology. Herein, we present experiments and simulations of the scattering morphology of a spherical particle. The morphology was probed as a function of particle size, incident beam polarization, and particle separation distance. We found that spherical particles scattered light with a non-circular morphology. Moreover, we found the morphology depended upon both the scaled particle size with respect to the incident beam wavelength and the incident beam polarization. Although the scattering morphology from the sphere was surprisingly complex, we did not find that these effects would alter the interpretation of scattering as a function of particle separation distance.

### 1. Introduction

Micrometer scale “colloidal” particles are regularly found in industrial and natural systems [1]. Microstructured chemical products, such as coatings, food, and lubricants, often include colloidal particles to impart specific chemical functions or mechanical properties. Product formulations are engineered to achieve a specific functionality [2]. Conservative interactions play a vital role in achieving that functionality. Specifically, the processing procedures, the storage protocols, and the performance of the applications involve suspensions of colloidal particles would critically depend upon the surface interactions between colloidal particles. For instance, the long-term stability of a coating that contains micrometer scale pigment particles depends critically on the conservative interactions operating between those pigment particles, and also between the pigment particles and solvent.

A variety of techniques have been developed over the past decades for measuring colloidal interactions. These include, but are not limited to, Atomic Force Microscopy (AFM) [3], Surface Force Apparatus (SFA) [4, 5], and Total Internal Reflection Microscopy (TIRM) [6, 7]. AFM and SFA depend on the manipulation of two

---

<sup>1</sup> Chemical and Biomedical Engineering, Cleveland State University, Cleveland, Ohio, USA.

<sup>2</sup> Deutsches Zentrum für Luft- und Raumfahrt (DLR), Institute of Remote Sensing, Weßling, Germany.

<sup>3</sup> Independent Researcher, Herrsching am Ammersee, Germany.

<sup>4</sup> Leibniz-Institut für Werkstofforientierte Technologien — IWT, University of Bremen, Bremen, Germany.

<sup>5</sup> Chemical and Biomolecular Engineering Department, Case Western Reserve University, Cleveland, Ohio, USA.

<sup>6</sup> Corresponding author; e-mail: clw22@case.edu.

approaching surfaces. Although robust, the sensitivity of this approach is limited by one's ability to mechanically manipulate those surfaces. TIRM does not rely on such an operation because this technique utilizes Brownian fluctuations to infer colloidal forces [8]. TIRM is able to measure weak  $\sim kT$  scale interactions by tracking these random fluctuations of a particle very near a boundary. Conventional TIRM works by tracking the light scattered from a fluctuating spherical particle near a boundary. The particle in an electrolyte would scatter light from the evanescent wave that propagates along the surface with an intensity that decays exponentially [9, 10]. The intensity of light scattered by a particle depends exquisitely on the height of the particle, thus by tracking the total integrated intensity of light scattered one can directly track the separation distance between the particle and the boundary. Conventional TIRM has been found in a broad range of applications for many systems over the last three decades [11–16].

One challenge with the application of conventional TIRM, however, is utilizing this technique with novel anisotropic particles [17]. Particles with a non-spherical shape or anisotropic optical properties will cause light scattered from the particle to depend upon not only the separation distance, but also its orientation with respect to the evanescent wave [18, 19]. Decoding the signature of this scattered light for a specific type of anisotropic particle is a current challenge that Scattering Morphology Resolved Total Internal Reflection Microscopy (SMR-TIRM) intends to address. SMR-TIRM uses the morphology of scattering in addition to the integrated intensity. Recent experimental and simulation results have shown that both the morphology and integrated intensity sensitively depend upon the orientation of an ellipsoidal colloid [18]. Primarily, this information could be used to estimate the orientation and position of the ellipsoid, thereby providing the necessary information to assemble the potential energy landscape for an anisotropic particle [20].

In addition, these experiments have revealed that SMR-TIRM could be used to probe the shape and orientation of fixed particles, synthetic or biological in nature. Recent work has even suggested the shape of adhered particles could be inferred from the morphology itself [21], but careful considerations are required when analyzing the scattering from a particle. For instance, the scattering morphology associated with a  $\sim \mu\text{m}$  scale particle is known to be displaced from the particle center with a shape that depends on the specific optical system being used to collect the scattering. Although most images of scattering morphology typically show a circular projected area of scattering from an isotropic particle, there has been no investigation of such phenomena. Realizing the use of SMR-TIRM to probe adhered particles, such as bacteria [22], requires a thorough understanding of how scattering morphology from an adhered particle depends on size and shape.

Herein, we conducted measurements and simulations on spherical particles with SMR-TIRM. Although initially meant as a comparison to validate the approach of SMR-TIRM, results from these benchmark studies on spheres revealed a surprising result that will be the focus of the manuscript. Namely, that the morphology of scattering from a sphere deviated from a circular projected area and the extent of this deviation depended upon particle size and incident beam polarization. We first describe SMR-TIRM experimental measurements and complementary simulations of isotropic spheres with systematic variation in size. These results suggested the extent to which morphology deviated from a circle, in which the aspect ratio (AR) of the projected area of scattering morphology is equal to one ( $AR = 1$ ), will depend upon the size of the particle. Furthermore, we explored how this effect would impact the integrated intensity of scattering. Similar to an ellipsoid particle, the non-circular projected morphology from a sphere found here had an integrated intensity that depended exponentially on the separation distance.

## 2. Materials and Methods

### 2.1. Scattering Morphology Resolved Total Internal Reflection Microscopy (SMR-TIRM) of Spheres.

Figure 1 shows the setup of Scattering Morphology Resolved Total Internal Reflection Microscopy (SMR-TIRM).

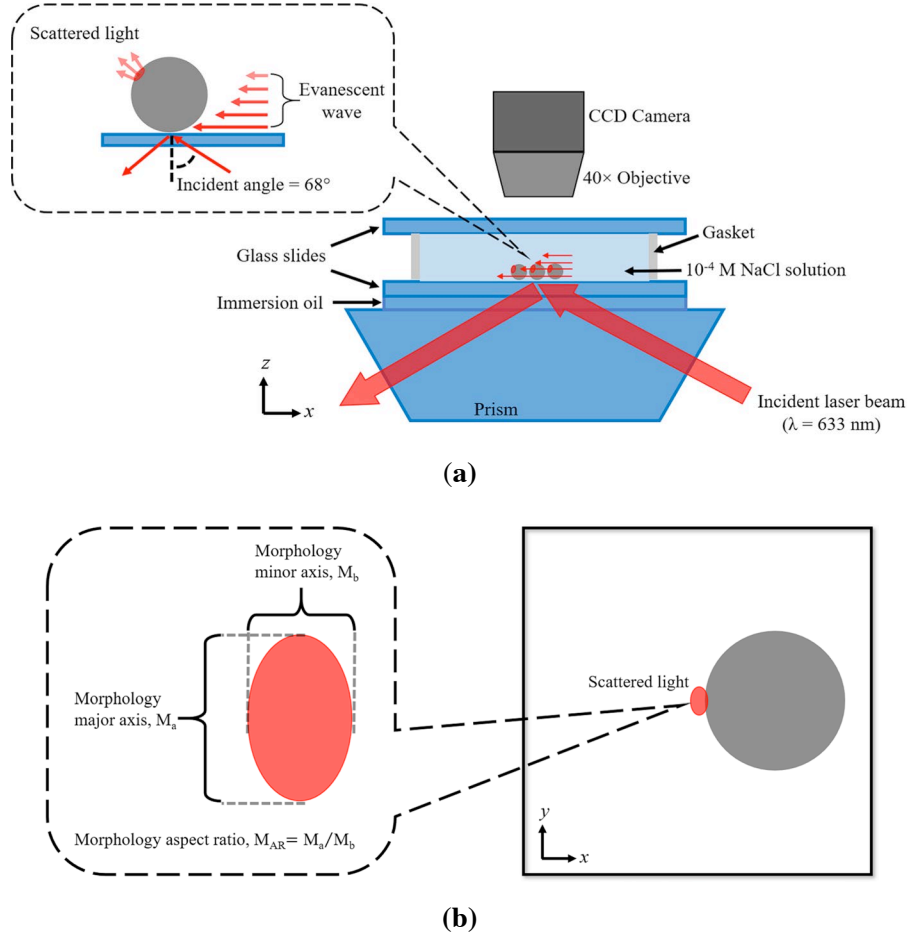


**Fig. 1.** Scattering Morphology Resolved Total Internal Reflection Microscopy (SMR-TIRM). (a) The apparatus consists of a beam with an incident angle above the critical angle as set by the materials comprising the interface. Nearby particles will scatter light with an integrated intensity that depends upon the separation distance; (b) SMR-TIRM is designed to measure and interpret the scattering morphology in addition to the integrated intensity.

It is based on an upright microscope system (Olympus BX51WI), and the light source is a 633 nm laser (PLM-633.0-PMF, NECSEL Co.), which has a single-mode 1-meter polarization maintaining optical fiber (NECSEL) coupled to an aspherical collimator (CFC-8X-A,  $f = 7.5$  mm, Thorlabs). The collimator is inserted into a 3D printed mount that also holds a linear polarizer (FBR-LPVIS 500 — 720 nm, Thorlabs) and a custom-made dove prism (BK7 glass, top facet:  $25 \times 50$  mm<sup>2</sup>, diagonal sides of  $68^\circ$  and  $75^\circ$ ). The polarizer was tuned to match with the polarization maintaining fiber such that the incident laser beam would be either s- or p- polarization. The experimental apparatus was fixed on a floating table to minimize the impact from mechanical vibrations.

The incident angle was set to be  $68^\circ$  for experiments described herein. Note for a glass-water ( $n_1 = 1.515$ ,  $n_2 = 1.33$ ) interface ( $\theta_c = 61^\circ$ ),  $68^\circ$  is larger than the theoretical critical angle to achieve total internal reflection. The laser power was set to 0.3 mW via the laser control software (Raman Boxx, NECSEL). The suspension of colloidal spheres (microparticles based on polystyrene, Sigma Aldrich) was placed inside a microfluidic cell, which was sandwiched by two 1 mm thick microscope slides with a gasket (120  $\mu$ m deep Secure-Seal<sup>TM</sup>, Invitrogen). Herein, we prepared two different microfluidic cells. One contained 3, 5, 10  $\mu$ m spheres, while the other contained 20 and 30  $\mu$ m spheres. The microfluidic cell was then optically coupled to the prism with refractive index matching oil (Resolve<sup>TM</sup>, Thermo Scientific,  $n = 1.515$ ). The particle number concentration was

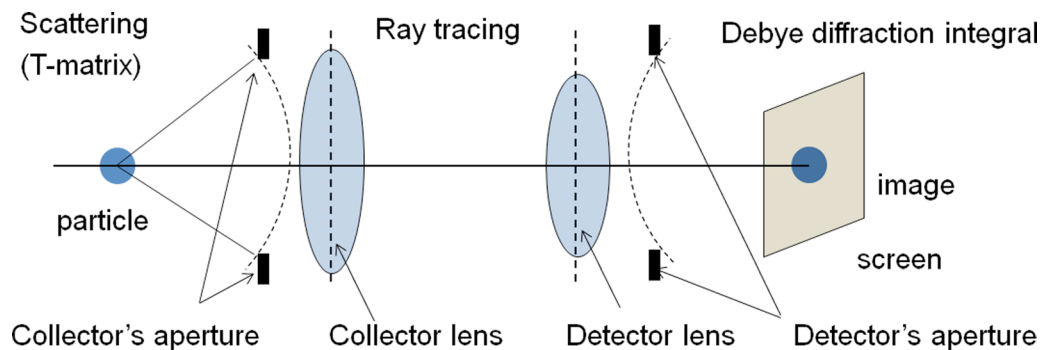


**Fig. 2.** Optical scheme for the particle visualization routine.

kept low enough within the region of interest to ensure the scattered light from different particles would not interfere with each other.

Scattered light from colloidal spheres attached to the glass wall was collected through a  $40\times$  microscope objective directly above the microfluidic cell (LUCPLFN40X,  $NA = 0.6$ , Olympus) and a camera (ORCA-Fusion, DIGITAL CAMERA C14440, Hamamatsu). Images with a size of  $100 \times 100$  pixels<sup>2</sup> were captured with an exposure time of 10 ms and an 8-bit depth unless indicated otherwise. The format of images was .tif without any compression or post-processing. A two-axis linear translation stage was used to find the evanescent wave illuminated region where the scattered light could be observed from colloidal spheres. In addition, a microscope lamp (Olympus U-LH100-3) served as the back-light source to locate the spheres on the glass wall.

**2.2. Simulations of SMR-TIRM.** Simulations were conducted herein to generate micrographs of scattering morphology to compare with experimental images. The algorithm for solving the scattering problem is well established [23–26] and the method for generating images has previously been described [19]. Briefly, this algorithm consists of a module for computing electromagnetic scattering field by axis-symmetric particles and the visualization subroutine. The computations of a scattering field are based on the T-matrix method applied for a particle that is near a plane surface. Although the model handles the scattering by a Janus axisymmetric particle of arbitrary orientation situated in the evanescent field near a plane surface, for current simulations, the homogeneous spherical particles are considered. The visualization tool is implemented for the optical scheme shown in Fig. 2. The scattered field on the Gaussian reference sphere of the collector lens is computed by means of the T-matrix method, while the transmitted field on the Gaussian reference sphere of the detector lens is computed by using the ray tracing technique. For focus field calculation, the Debye diffraction integral is applied. The obtained image is then cropped and filtered by setting to zero the pixel brightness if it is less than a threshold value (which is set to 0.001 from the maximum pixel brightness of the image).

Scattering morphology was collected for spherical particles of systematic variation in size and with either s- or p- incident polarization at a fixed azimuthal angle. Figure 3 shows micrographs from both bright field and SMR-TIRM imaging. Inspection of these images reveals multiple important features. First, the centers of all morphologies were displaced from the center of the particle, again suggesting the intensity variation of the morphology in the focal plane could not directly be used to infer the curvature of the particle. Moreover, the typical length scale of the scattering morphology did not change substantially as the particle grew in size. Further, although there were conditions (diameter  $< 10$  nm) in which scattering was observed to have nearly a circular projected area as expected, particles with a diameter  $\geq 10$  nm had a non-circular morphology. Qualitatively, the morphology appeared to deviate from the circular shape as the diameter of the spherical particle increased. Finally, there were slight differences in morphology as a function of incident polarization. These experimental

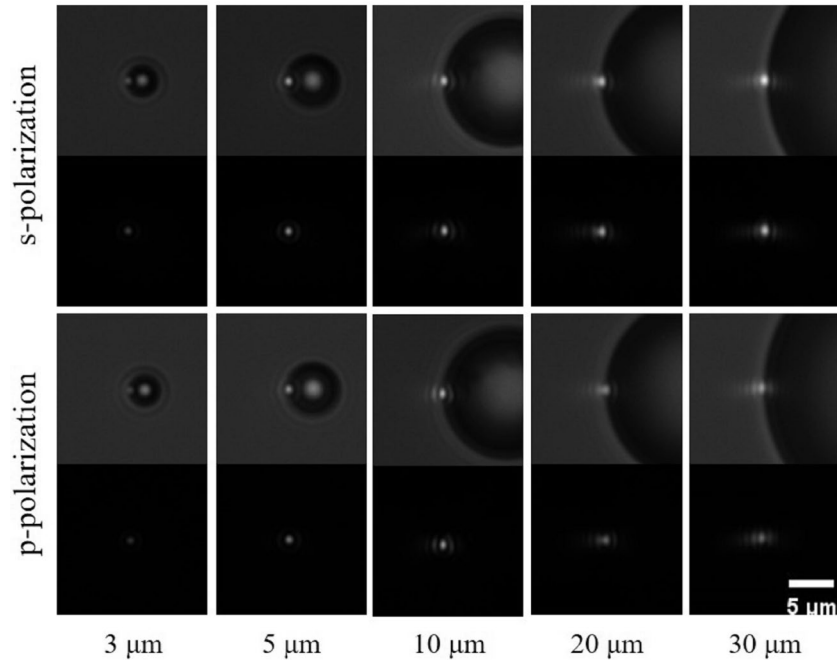


**Fig. 3.** Brightfield and SMR-TIRM experimental micrographs of spheres for s- and p-polarization. Bright field illumination and SMR-TIRM was used to probe particles displayed in the top panel for each polarization, while only SMR-TIRM was used in the images on the bottom panel. Visual inspection reveals that particles with a diameter  $< 10$  mm tended to scatter light with a circular projected area displaced from the center. However, particles with diameters  $\geq 10$  mm had a scattering morphology, still displaced from the center, deformed from a circular projected area. Moreover, the typical length scale of the scattering morphology did not grow substantially in size with particle size.

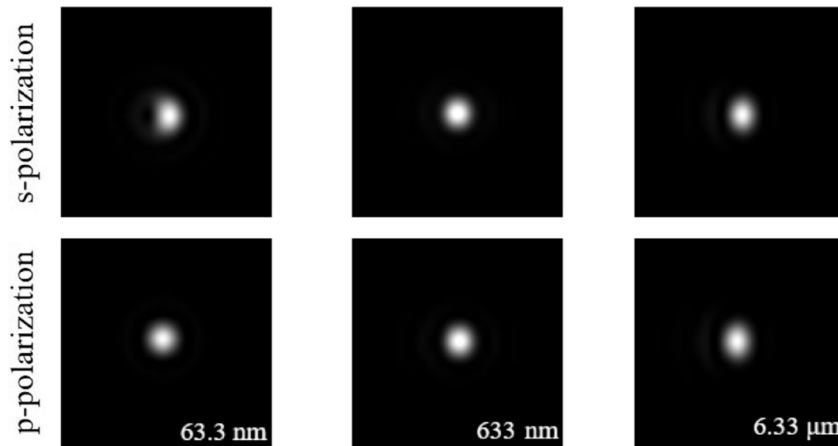


**Fig. 4.** SMR-TIRM simulated micrographs of spheres for s- and p-polarization. Similar to the experimental micrographs, there was a slight deviation from circular projected area as the particle diameter was increased. Note the particle size regime used for simulations herein was smaller than that of experimental measurements, with some overlap between the two. The simulation tool reliably converges for particle diameters  $\leq 15$  nm.

measurements were complemented with simulations at conditions in which the particle size was systematically varied in size with respect to the incident beam wavelength  $a/\lambda$ . The quotient  $a/\lambda$  was varied from 0.1 to 10 and the incident polarization was set to either s- or p- polarization. Similar to the observations made in the experimental measurements, we found the morphology aspect ratio to deviate from a circular projected area (see Fig. 4).

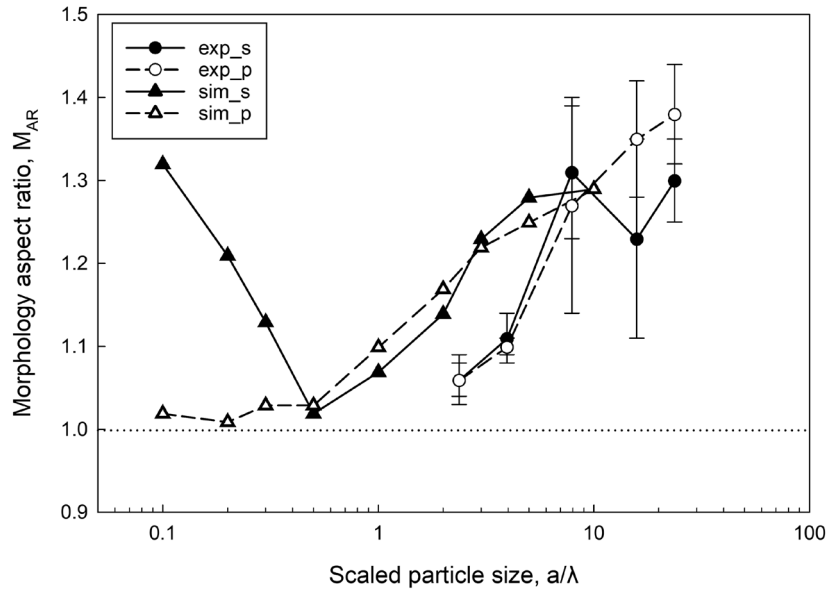


**Fig. 5.** Morphology aspect ratio ( $M_{AR}$ ) from experimental and simulated SMR-TIRM micrographs. Particles were systematically varied in size with respect to the incident beam wavelength. The  $M_{AR}$  tended to increase for spherical particles with increasing size for  $a/\lambda \geq 0.5$ . However, there was a distinct difference in scattering morphology between the two polarizations for simulated images where  $a/\lambda < 0.5$ . The s-polarization (the electric field in the direction perpendicular to the substrate) tended to have a morphology aspect ratio that decreased as particle size increased. However, p-polarization (the electric field in the direction parallel to the substrate) remained at a morphology aspect ratio near  $\sim 1$ .

### 3. Results and Discussion

The scattering morphology from these particles was analyzed via fitting a two-dimensional Gaussian profile as is done for colloidal ellipsoids [18]. We found simulations and experiments both suggested at  $a/\lambda \geq 0.5$ , the morphology aspect ratio,  $M_{AR}$ , would increase from a value of  $\sim 1.0$  to  $\sim 1.3$  for s- and p- polarizations as  $a/\lambda$  increased (see Fig. 5). Besides, there was a strong dependence of  $M_{AR}$  on the polarization at  $a/\lambda < 0.5$ . In the simulated micrographs,  $M_{AR}$  maintained  $\sim 1.0$  for incident polarization of p-, while  $M_{AR}$  would change dramatically for s-polarization at those same conditions. Specifically,  $M_{AR}$  reached  $\sim 1.3$  at  $a/\lambda = 0.1$  and then started to approach  $\sim 1.0$  as  $a/\lambda$  gradually increased from 0.1 to 0.5.

One critical feature of both TIRM and SMR-TIRM is the dependence of integrated intensity on the separation distance. Deviation from exponential dependence of integrated intensity, a consequence of  $M_{AR}$  diverging from  $= 1$ , as a function of separation distance would significantly alter the way in which raw data is analyzed. Herein, we probed the dependence of integrated intensity on particle size and separation distance by simulating the scattering morphology for a particle with  $M_{AR} > 1$  at systematically varied separation distances. Figure 6 shows the integrated scattering intensity as a function of particle height from the simulations for spheres with a diameter of 6.33  $\mu\text{m}$ .

These data confirm the integrated scattering intensity exponentially decays with increasing separation distance from the wall, even at  $M_{AR} > 1$ . In addition, the two sets of data each have a slope  $-\beta$ , which agrees with the penetration depth of the evanescent wave intensity ( $\beta^{-1} = 0.11$   $\mu\text{m}$ ),  $\beta = \frac{4\pi}{\lambda} \sqrt{(n_1 \sin \theta_i)^2 - n_2^2}$ , where  $\lambda$  is the wavelength of the incident laser beam,  $\theta_i$  is the incident angle,  $n_1$  and  $n_2$  are the refractive indexes of glass and water, respectively.

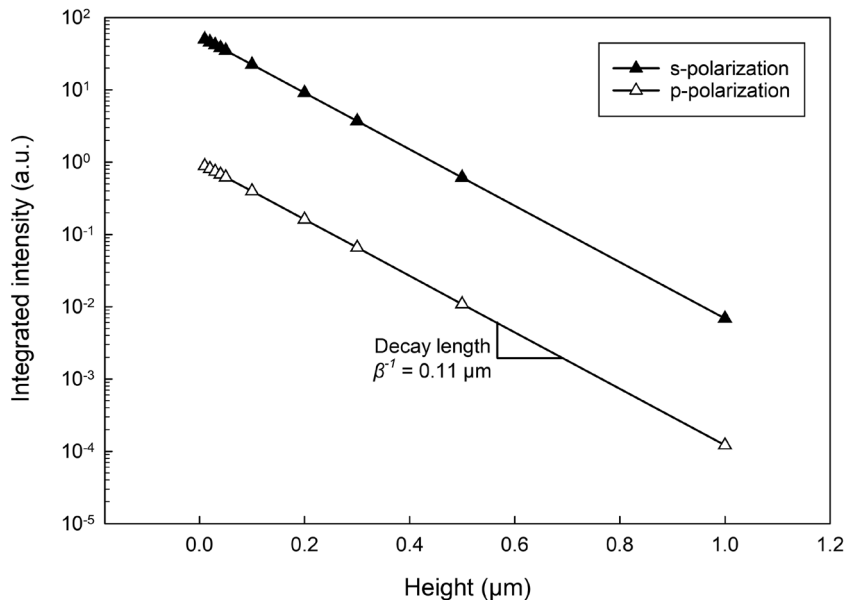


**Fig. 6.** Integrated intensity for spheres with systematic variation in separation distance. The integrated intensity of scattering morphology depended on separation distance as expected, despite the variation of morphology shape.

#### 4. Conclusions

Experiments and simulations of Scattering Morphology Resolved Total Internal Reflection (SMR-TIRM) were used to probe the morphology of scattered light from a spherical particle adhered to a boundary. Beyond benchmarking for the new technique of SMR-TIRM, the work summarized herein supplements our existing understanding of scattering morphology dependence on particle size, shape, and beam polarization. We found the scattering morphology, displaced from the center of the particle, to have a morphology aspect ratio  $M_{AR}$  depends on both particle size and incident polarization. However, the integrated intensity remained exponentially dependent on the separation distance for  $M_{AR} > 1$ . We conclude from these findings one cannot assume the circular projected area is directly cast from the spherical shape of the particle.

This work was supported by the National Science Foundation CAREER Award, No. 1752051.

This manuscript was submitted as part of the Lomonosov Readings 2020, Section: Mathematical models and methods in electromagnetics for particles simulations, characterization and synthesis (December 2020).

#### REFERENCES

1. J. C. Berg, *An Introduction to Interfaces and Colloids*, 1st ed., World Scientific (2009).
2. L. Kavanagh and P. Lant, "Introduction to chemical product design," *Educ. Chem. Eng.*, **1**, 66 (2006).
3. P. M. Claesson, T. Ederth, V. Bergeron, and M. W. Rutland, "Techniques for measuring surface forces," *Adv. Colloid Interface Sci.*, **67**, 119 (1996).
4. Y. Wang, G. A. Pilkington, C. Dhong, and J. Frechette, "Elastic deformation during dynamic force measurements in viscous fluids," *Curr. Opin. Colloid Interface Sci.*, **27**, 43 (2017).
5. J. Israelachvili, Y. Min, M. Akbulut, A. Alig, G. Carver, W. Greene, K. Kristiansen, E. Meyer, N. Pesika, K. Rosenberg, and H. Zeng, "Recent advances in the surface forces apparatus (SFA) technique," *Reports Prog. Phys.*, **73**, 036601 (2010).

6. D. C. Prieve, "Measurement of colloidal forces with TIRM," *Adv. Colloid Interface Sci.*, **82**, 93 (1999).
7. M. A. Bevan and S. L. Eichmann, "Optical microscopy measurements of KT-scale colloidal interactions," *Curr. Opin. Colloid Interface Sci.*, **16**, 149 (2011).
8. D. S. Sholl, M. K. Fenwick, E. Atman, and D. C. Prieve, "Brownian dynamics simulation of the motion of a rigid sphere in a viscous fluid very near a wall," *J. Chem. Phys.*, **113**, 9268 (2000).
9. D. C. Prieve and N. A. Frej, "Total internal reflection microscopy: a quantitative tool for the measurement of colloidal forces," *Langmuir*, **6**, 396 (1990).
10. D. C. Prieve and J. Y. Walz, "Scattering of an evanescent surface wave by a microscopic dielectric sphere," *Appl. Opt.*, **32**, 1629 (1993).
11. R. M. Rock, P. J. Sides, and D. C. Prieve, "Ensemble average TIRM for imaging amperometry," *J. Colloid Interface Sci.*, **403**, 142 (2013).
12. T. D. Edwards and M. A. Bevan, "Depletion-mediated potentials and phase behavior for micelles, macromolecules, nanoparticles, and hydrogel particles," *Langmuir*, **28**, 13816 (2012).
13. S. Biggs, R. R. Dagastine, and D. C. Prieve, "Oscillatory packing and depletion of polyelectrolyte molecules at an oxide — water interface," *J. Phys. Chem. B*, **106**, 11557 (2002).
14. X. Gong, Z. Wang, and T. Ngai, "Direct measurements of particle–surface interactions in aqueous solutions with total internal reflection microscopy," *Chem. Commun.*, **50**, 6556 (2014).
15. C. L. Wirth, P. J. Sides, and D. C. Prieve, "The imaging ammeter," *J. Colloid Interface Sci.*, **357**, 1 (2011).
16. J. A. Fagan, P. J. Sides, and D. C. Prieve, "Vertical oscillatory motion of a single colloidal particle adjacent to an electrode in an ac electric field," *Langmuir*, **18**, 7810 (2002).
17. S. C. Glotzer and M. J. Solomon, "Anisotropy of building blocks and their assembly into complex structures," *Nat. Mater.*, **6**, 557 (2007).
18. A. Rashidi, S. Domínguez-Medina, J. Yan, D. S. Efremenko, A. A. Vasilyeva, A. Doicu, T. Wriedt, and C. L. Wirth, "Developing scattering morphology resolved total internal reflection microscopy (SMR-TIRM) for orientation detection of colloidal ellipsoids," *Langmuir*, **36**, 13041 (2020).
19. A. Doicu, A. A. Vasilyeva, D. S. Efremenko, C. L. Wirth, and T. Wriedt, "A light scattering model for total internal reflection microscopy of geometrically anisotropic particles," *J. Mod. Opt.*, **66**, 1139 (2019).
20. A. Rashidi and C. L. Wirth, "Motion of a janus particle very near a wall," *J. Chem. Phys.*, **147**, 224906 (2017).
21. A. Xia, S. Yang, R. Zhang, L. Ni, X. Xing, and F. Jin, "Imaging the separation distance between the attached bacterial cells and the surface with a total internal reflection dark-field microscope," *Langmuir*, **35**, 8860 (2019).
22. G. C. L. Wong, J. D. Antani, P. Lele, J. Chen, B. Nan, M. J. Kühn, A. Persat, J.-L. Bru, N. M. Høyland-Kroghsbo, A. Siryaporn, J. Conrad, F. Carrara, Y. Yawata, R. Stocker, Y. Brun, G. Whitfield, C. Lee, J. de Anda, W. C. Schmidt, R. Golestanian, G. A. O'Toole, K. Floyd, F. Yildiz, S. Yang, F. Jin, M. Toyofuku, L. Eberl, N. Nobuhiko, L. Zacharoff, M. Y. El-Naggar, S. E. Yalcin, N. Malvankar, M. D. Rojas-Andrade, A. Hochbaum, J. Yan, H. A. Stone, N. S. Wingreen, B. Bassler, Y. Wu, H. Xu, K. Drescher, and J. Dunkel, "Roadmap on emerging concepts in the physical biology of bacterial biofilms: from surface sensing to community formation," *Phys. Biol.* (2021).
23. T. Wriedt, "Using the T-matrix method for light scattering computations by non-axisymmetric particles: superellipsoids and realistically shaped particles," *Part. Part. Syst. Character.*, **19**, 256 (2002).
24. N. Riefler, E. Eremina, C. Hertlein, L. Helden, Y. Eremin, T. Wriedt, and C. Bechinger, "Comparison of T-matrix method with discrete sources method applied for total internal reflection microscopy," *J. Quant. Spectrosc. Radiat. Transf.*, **106**, 464 (2007).
25. G. Gouesbet and J. a Lock, "Journal of quantitative spectroscopy & radiative transfer on the electromagnetic scattering of arbitrary shaped beams by arbitrary shaped particles : a review," *J. Quant. Spectrosc. Radiat. Transf.*, **162**, 1 (2014).
26. A. Doicu, T. Wriedt, and Y. A. Eremin, *Light Scattering by Systems of Particles, Null-Field Method with Discrete Sources* (2006).